

Phoenix Mars Scout Parachute Flight Behavior and Observations

Douglas S. Adams
Jet Propulsion Laboratory
4800 Oak Grove Drive
Pasadena, CA 91109
818-393-6387
Douglas.S.Adams@jpl.nasa.gov

Allen Witkowski and Mike Kandis
Pioneer Aerospace Corporation
45 South Satellite Road
South Windsor, CT 06074
860-528-0092
Al.Witkowski@zodiacaerospace.com
Mike.Kandis@zodiacaerospace.com

Abstract—The data returned from the successful Phoenix Mars Scout mission are analyzed in order to determine characteristics and behaviors of the supersonic parachute that was used to slow the entry body during its descent to the surface. At least one significant drag reduction event was observed when the vehicle was traveling at Mach 1.6; this is consistent with previously reported terrestrial high altitude testing and is likely associated with an area oscillation of the parachute. The parachute is shown to possess some lateral instability relative to the anti-velocity vector that is also at a level that is consistent with the same historic data. Ramifications of the lateral instability and, in particular, the unsteadiness in the parachute drag are discussed as energizing elements of the entry body wrist mode. The apparent coefficient of drag for the parachute is calculated and shown to have relatively small variations on an average basis over the supersonic portion of flight.^{1,2}

TABLE OF CONTENTS

1. INTRODUCTION	1
2. THE MRO IMAGE	1
3. PARACHUTE DRAG DATA	2
4. PARACHUTE LATERAL STABILITY	4
5. CONCLUSIONS	7
REFERENCES	7
BIOGRAPHY	7

1. INTRODUCTION

The Phoenix Mars Scout (MSP) parachute deployed and functioned nominally during entry, descent and landing (EDL) at Mars on May 25, 2008, leading to a successful landing on the Martian northern plains. The on-board inertial measurement unit (IMU) data were recorded at 200 Hz during the entire EDL sequence and relayed to Earth following landing. This represents, by more than an order of magnitude, the best measurement of any Mars entry

vehicle dynamics ever recorded. The data is analyzed to determine the Viking scaled 11.8 m reference diameter (D_0) disk-gap-band (DGB) parachute's behavior including its drag performance and lateral stability, as well as the combined effect of these, on the entry body attitude dynamics. In addition to the IMU data, Phoenix was also fortunate enough to benefit from a first of its kind image of the entry body on parachute taken by the High Resolution Imaging Science Experiment (HiRISE) camera on-board the Mars Reconnaissance Orbiter (MRO) during entry. This image is correlated with the IMU data to determine the flight regime at the time the image was captured.

2. THE MRO IMAGE

The photo of Phoenix taken by MRO is shown in Fig. 1. Because HiRISE is a push-broom type camera this allows the time the image was taken to be known with some degree of precision. In correlating the data sets it was determined that the image was taken 46.9 seconds after mortar fire when the entry vehicle was at an altitude of 9.2 km above ground level (AGL) and traveling at a near terminal velocity of 76 m/s (170 mph).

The HiRISE image has a resolution of about 40 cm per pixel and the Sun is illuminating roughly along the line of site so the view is excellent. Nevertheless, when the HiRISE image in Fig. 1 is compared to profile photographs of the Phoenix parachute taken during a low altitude drop test (LADT), as shown in Fig. 2, it is apparent that the band is notably more difficult to see. This is particularly true of the left and right portions of the band in Fig. 1. This shape bears a striking resemblance to the shadowgraphs of a 4% scaled Mars Science Laboratory (MSL) supersonic wind tunnel test shown in Fig. 3 [1]. However, given that the Fig. 1 image was taken in near steady state conditions at relatively low speeds, it is extremely unlikely that the parachute was imaged during an area oscillation and it is believed that the camera resolution and viewing angle

¹978-1-4244-7351-9/11/\$26.00 ©2011 IEEE.

²IEEEAC paper #1534, Version 10, Updated January, 11, 2011

effects have simply resulted in a blurring of the band in these areas. Additional analysis of the HiRISE image is available in Ref. 2.



Figure 1 – Phoenix parachute and entry body as photographed by MRO 46.9 seconds after deployment at an altitude of 9.2 km AGL and a velocity of 76 m/s.

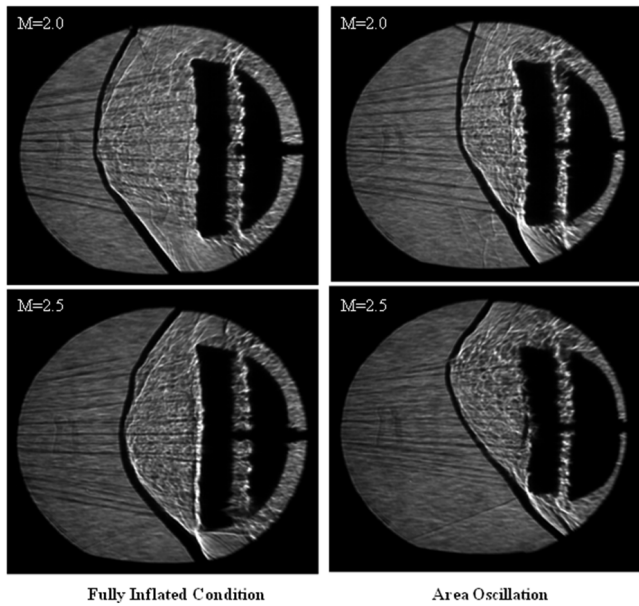


Figure 3 – Shadowgraphs of a 4% scale MSL parachute taken during supersonic wind tunnel testing [1]

3. PARACHUTE DRAG DATA

The reconstructed Mach number as a function of time for the 30 second period following the parachute mortar fire is shown in Fig. 4. The magnitude of the entry body sensed

acceleration is shown in Fig. 5 for the first five seconds immediately after mortar fire with a peak reported acceleration of 8.72 g's. The mortar was triggered at Mach 1.68 and the vehicle continued to slow at just under one g for about one second before the parachute inflated. The actual inflation event took place in only 0.365 seconds from the time of line stretch to full-open which is easily the fastest opening time of any parachute used at Mars to date [3]. This quick opening is likely due to the Phoenix parachute's relatively small size (11.8 m) which is 70% the size of the Mars Exploration Rover (MER) parachute (14.1 m) and 54% the size of the Viking parachute (16.1 m).



Figure 2 – Phoenix parachute photographed during low altitude drop testing

In order to examine the parachute drag, it is first necessary to remove the drag generated by the entry body. This is done by characterizing the entry body drag over the period immediately prior to mortar fire and removing that acceleration from the subsequent data. The fruits of this effort are shown in Figs. 6 and 7 where the parachute drag force is plotted against time and Mach number respectively.

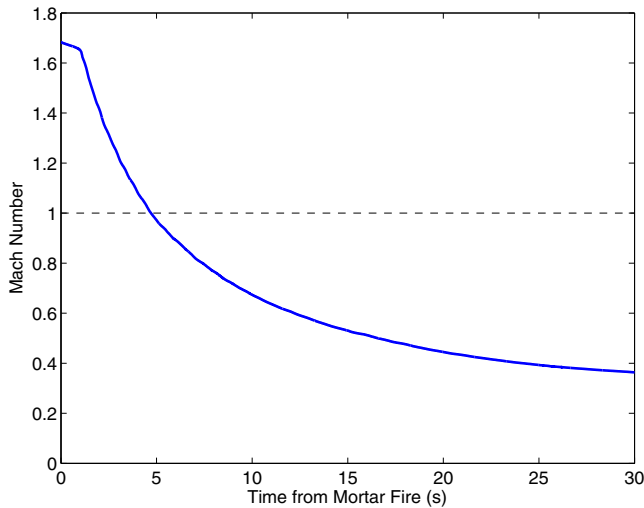


Figure 4 – Mach number as a function of time from parachute mortar fire

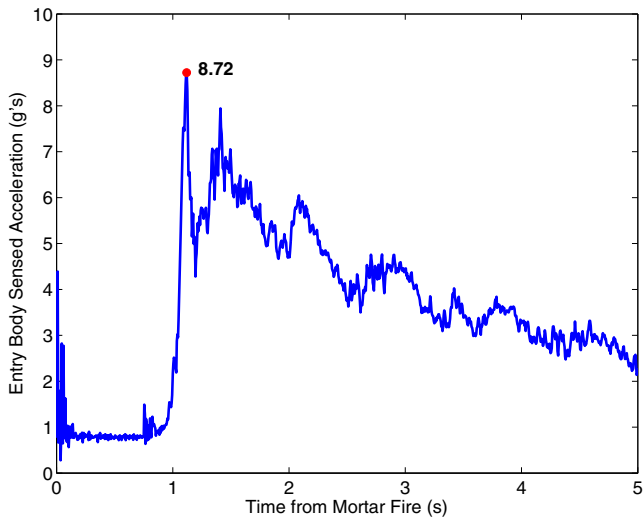


Figure 5 – Entry body sensed acceleration following parachute mortar fire

A few important observations can be readily made from Figs. 6 and 7. First, the mortar reaction load is evident at $t=0$ in Fig. 6. This is followed by the line stretch event at 0.8 seconds where the parachute canopy is extracted from the deployment bag and quickly inflates. Also, following the initial peak in drag force there is a sharp $\sim 50\%$ drop in drag which is attributed to an area oscillation although this cannot be confirmed in the absence of video data. Finally, as shown in both Figs. 6 and 7, the parachute drag remains

somewhat unsteady down to Mach 1.1, although there are no further significant drag loss events.

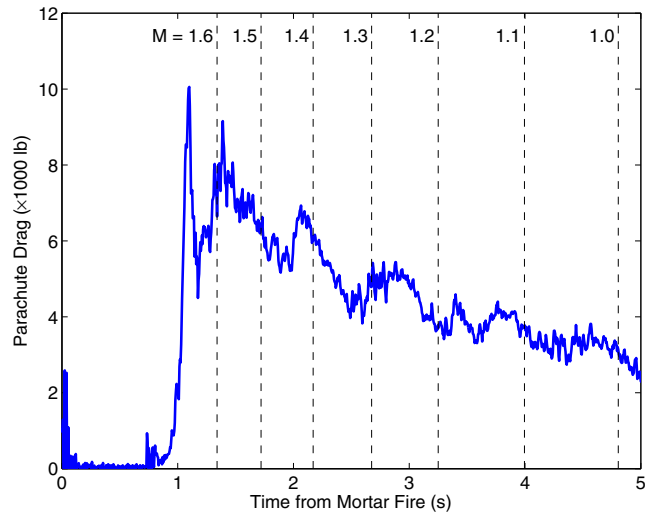


Figure 6 – Phoenix parachute drag force data immediately following parachute mortar fire where the Mach number is indicated with the vertical dashed lines

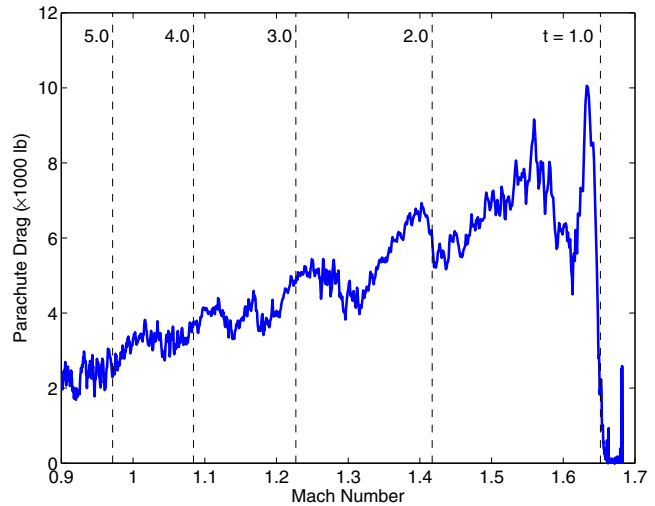


Figure 7 – Parachute drag as a function of Mach number where the time from parachute mortar fire is indicated with the vertical dashed lines

Although there is a clear and moderately deep drag reduction at 1.2 seconds, this feature is not repeated at lower speeds. This is consistent with terrestrial high altitude data obtained in support of the Viking missions from the Balloon Launched Decelerator Test (BLDT) AV-4 vehicle, shown in Fig. 8, which showed significant drag variability at speeds above Mach 1.5 [4]. The Phoenix entry vehicle slowed below Mach 1.5 quickly and only experienced the one major drag reduction event.

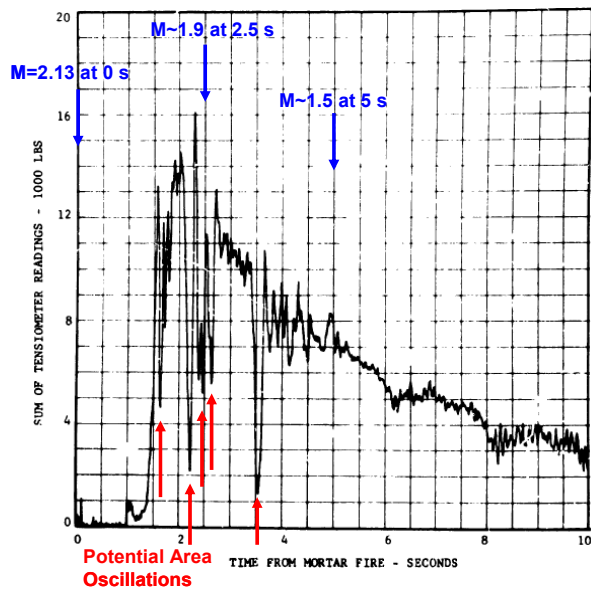


Figure 8 – Measured load history for BLDT AV-4 that shows unsteady drag with sharp drop-outs representing potential area oscillations at speeds above Mach 1.5 [4]

Finally, the parachute’s coefficient of drag (C_D) was calculated using the parachute drag force data from Fig. 6 in concert with the carefully reconstructed atmospheric density profile. The result of this analysis is shown in Fig. 9 where it is compared with the average subsonic C_D measured during a battery of terrestrial tests on Viking scaled parachutes. Owing to the unsteadiness of the data itself there are some variations evident in the C_D data, but these are to be expected and the values fall well within the ranges reported by other flight vehicles. It should be noted that neither the BLDT nor the Phoenix data indicate a reduction in drag at transonic speeds.

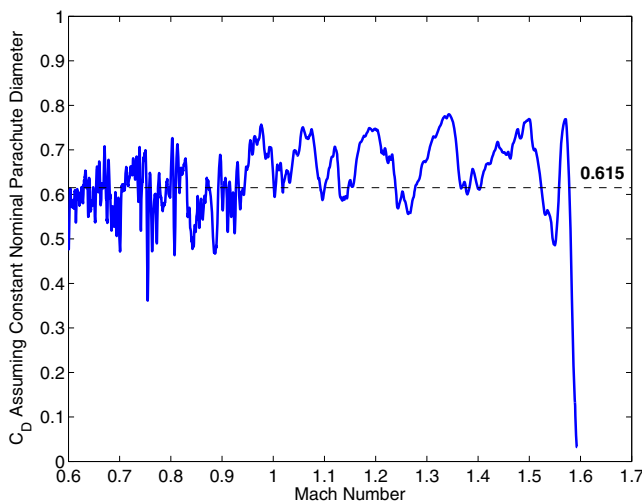


Figure 9 – Parachute C_D as a function of Mach number calculated assuming a constant nominal parachute diameter; the terrestrial low altitude drop test C_D of 0.615 is shown as the dashed line for reference

4. PARACHUTE LATERAL STABILITY

One of the most important results made possible by the high rate IMU data is a detailed examination of the parachute’s lateral dynamics at supersonic speeds. In order to affect this analysis it is first necessary to establish a relevant frame of reference for the parachute motion. This was done in the present study by defining an orthonormal set of unit vectors where the $+x$ direction is aligned with the entry body velocity, the $+z$ direction (\sim east) is defined through the cross-product of the velocity vector with the Mars rotation axis (the north pole) $\hat{z} = \hat{x} \times \hat{n}$, and the $+y$ direction (\sim north) is found from the cross-product of the first two vectors $\hat{y} = \hat{z} \times \hat{x}$. While this is strictly not a Newtonian reference frame it is found to be very close to one for the high velocity period of interest where the lateral velocities are tiny when compared to the entry vehicle’s supersonic speed.

Plots of the drag vector relative to the anti-velocity direction in this constructed frame are shown in Figs. 10 and 11 for the north-south and east-west motions respectively. The value of these data is more evident when they are combined in Fig. 12 to show the lateral motion of the parachute as observed from the entry vehicle looking upward.

Three important observations can be made from the data in Figs. 10-12. First, the parachute does not trim at a specific angle of attack but, instead, displays behavior more consistent with a neutral stability near the anti-velocity axis where the entry body wake is the strongest. Second, the parachute does not cone about the velocity axis but, rather, embarks on radial excursions away from and returning to the anti-velocity axis on nearly the same paths. And third, the amplitude of the motion is relatively small with peak angles generally remaining below eight degrees.

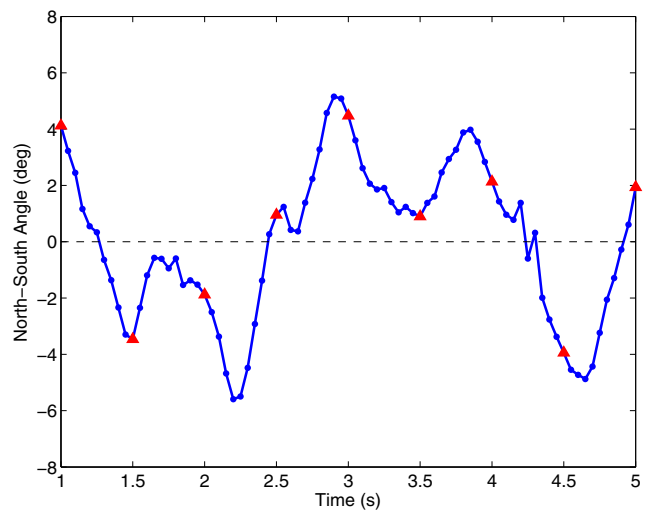


Figure 10 – Parachute velocity relative drag angle in the north-south direction (red triangles at 0.5 s intervals)

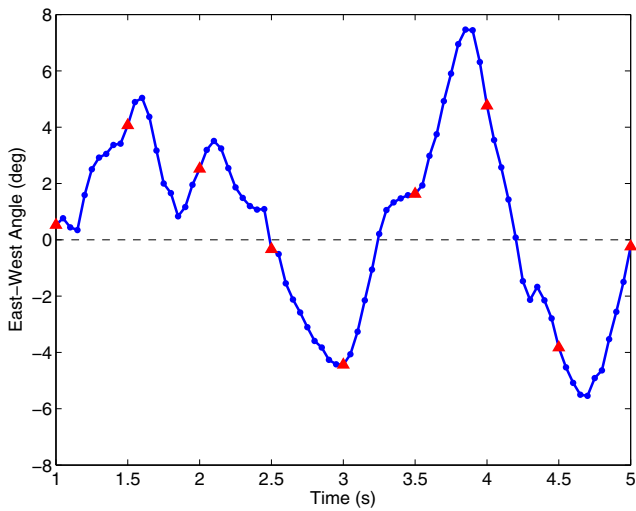


Figure 11 – Parachute velocity relative drag angle in the east-west direction (red triangles at 0.5 s intervals)

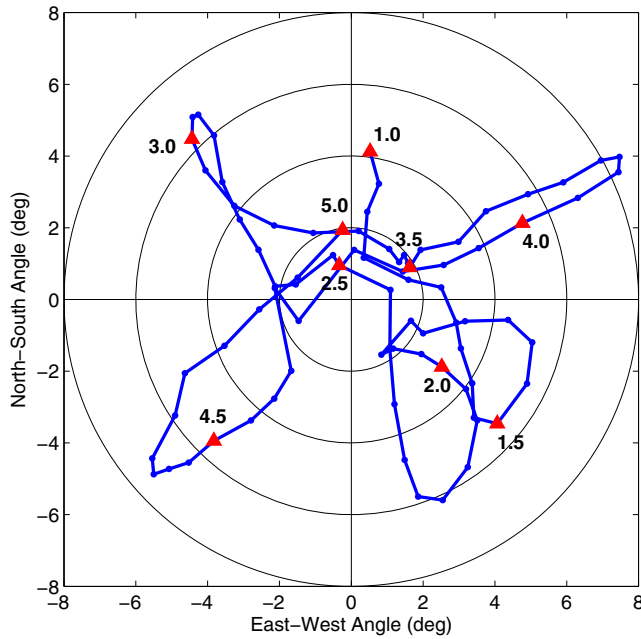


Figure 12 – Parachute velocity relative drag as viewed along the anti-velocity vector with labels at 0.5 second time intervals

It is also of interest to investigate the combined drag and lateral motion to see if there are correlated. To this end the parachute drag is plotted against the drag vector angle in Fig. 13. Two observations are made from this data. First, the drag reduction that occurs between 1.2 and 1.5 seconds coincides with a lateral translation away from the anti-velocity axis of approximately 4 degrees. Second, the lateral excursions are actually lower at higher Mach numbers with a trend towards increasing in amplitude (or at least maintaining approximately the same amplitude) at lower Mach numbers.

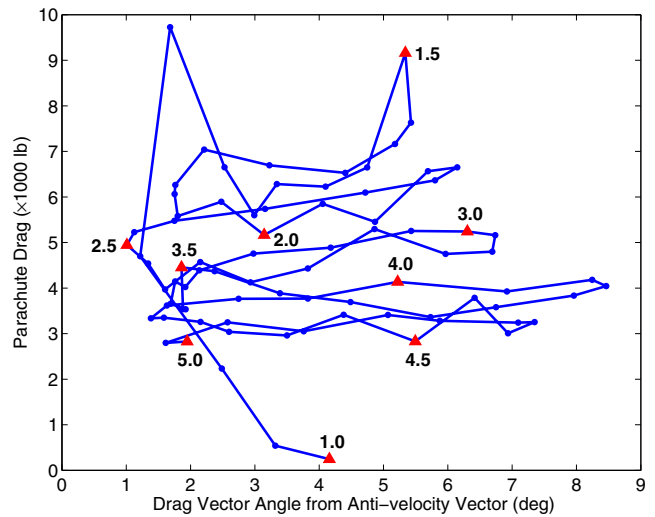


Figure 13 – Parachute drag versus the drag vector angle with respect to the anti-velocity vector (red triangles at 0.5 s intervals)

The unsteady drag and lateral motions of the parachute act to excite the angular motions of the entry body suspended below it. These motions are dominated by the wrist mode angular rates which are shown in Fig. 14. Some additional discussion is also available in Ref. 5. It should be noted that the peak angular rate of 100.2 deg/s does not occur until 3.6 seconds after parachute deployment and not immediately following parachute deployment as one would expect for a smooth parachute drag response.

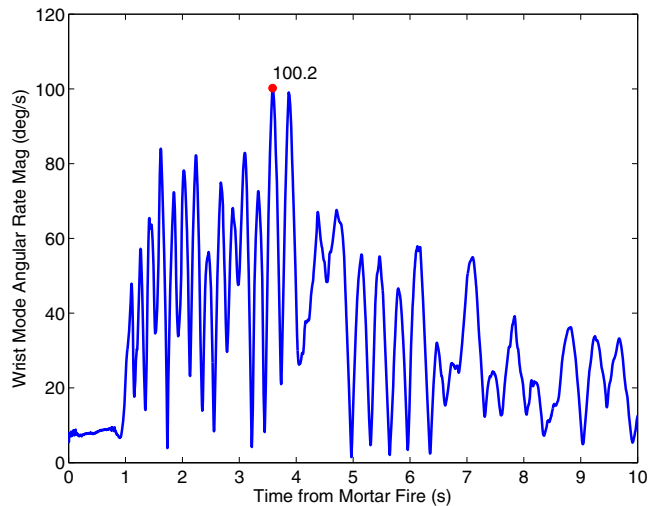


Figure 14 – Phoenix entry body wrist mode total angular rate magnitude following parachute mortar fire

It is also clear that there is a non-drag related event that significantly alters the wrist mode dynamics in Fig. 14 at 4.2 seconds after parachute deployment. It is likely that this is the result of lateral parachute motion seen in Figs. 10-12. Other investigations done for MSL have found that much of

the energy pumped into the wrist mode can be attributed to the drag instability of the parachute [6].

The parachute lateral stability was also examined at the lower Mach numbers immediately prior to backshell separation. The entry body angles to the local vertical (Nadir) are plotted in Fig. 15 where the angle is projected in the north-south and east-west directions to better illustrate the overall vehicle's performance. Because the period of the wrist mode motion is significantly shorter than the periods of motions shown in Fig. 15, the attitude of the entry vehicle itself can be taken as a good indicator of the parachute's relative orientation. The data in Fig. 15 again display behavior consistent with a neutral stability with excursions in angle of attack but with no stable trim angles.

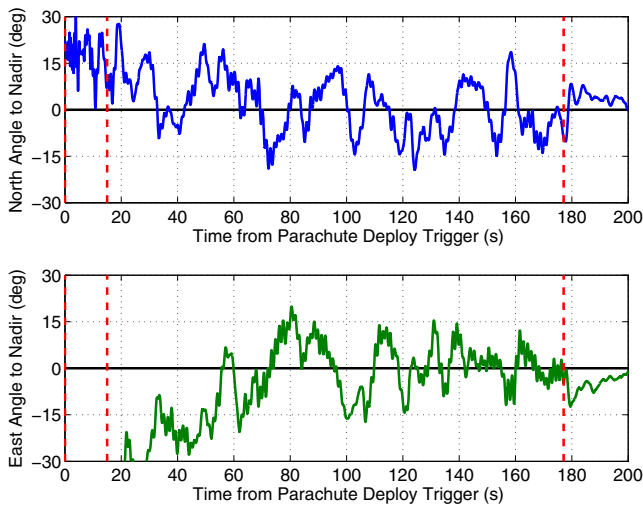


Figure 15 – Phoenix entry body angles to local vertical (Nadir) following parachute mortar fire where the heatshield and backshell separations are indicated by the vertical dashed red lines

The entry body velocity in the Mars Relative Descent (MRD) Local Vertical, Local Horizontal Coordinate System is shown in Fig. 16. The MRD frame is a north-east-down orthonormal frame that tracks the local vertical at all times and is a particularly useful frame for describing the entry dynamics. The velocity data in Fig. 16 suggests that, over roughly the final 60 seconds on the parachute (prior to backshell separation), the vehicle was drifting to the east at about 10 m/s and to the south at about 5 m/s. This is also evident from the plot of the ground track in Fig. 17 which shows the lander's position relative to the landing site where the track to the east-southeast is apparent.

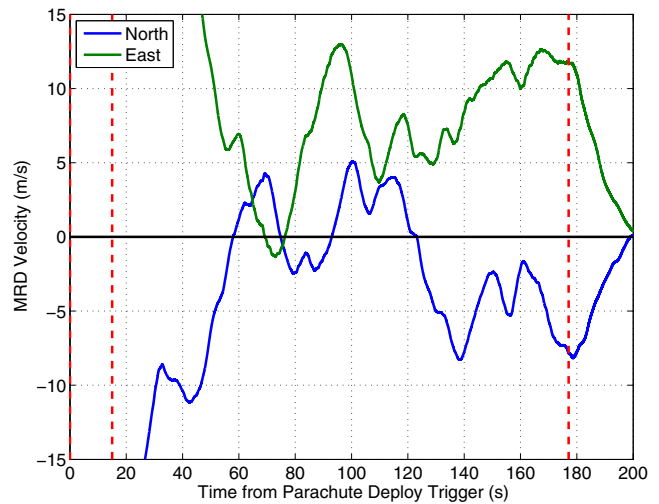


Figure 16 – Phoenix entry body velocity in the MRD frame following parachute mortar fire where the heatshield and backshell separations are indicated by the vertical dashed red lines

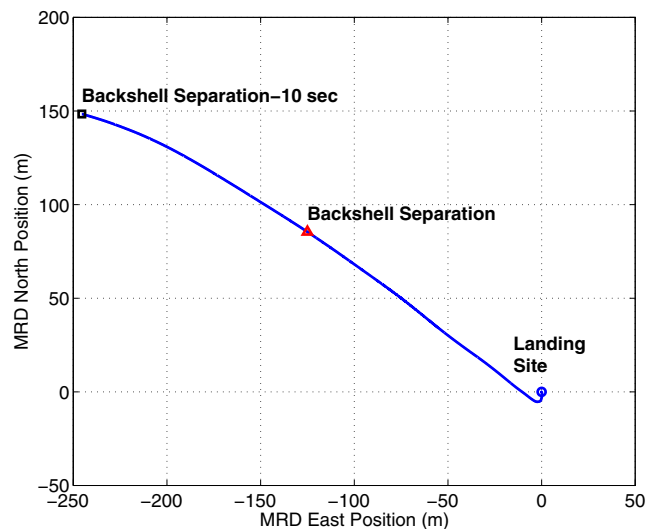


Figure 17 – Phoenix entry body position in the MRD frame from 10 seconds prior to backshell separation through landing

To further explore the terminal descent dynamics the entry body's attitude with respect to the local vertical is plotted over the final 10 seconds immediately prior to backshell separation in Fig. 18. The angles in Fig. 18 are calculated such that they indicate the direction of the parachute relative to the entry body in the MRD sense thus, if the parachute angle is to the south, then the force it is generating is acting to accelerate the vehicle to the south.

It is clear from Fig. 18 that the parachute is not flying in a stable trim condition. In fact, when the data presented in Figs. 15-18 are considered as a whole, the authors conclude that it is likely the Phoenix entry body was descending nearly vertically through an air mass that was moving

approximately 10 m/s to the east-southeast during its terminal decent. It should be noted that if the attitude and MRD velocity alone are used to estimate the parachute's angle of attack then, due to the presence of this wind velocity, an erroneous angle of attack will result wherein the vehicle will appear to maintain a steady lifting direction. However, the attitude history of the vehicle does not support a stable parachute trim angle.

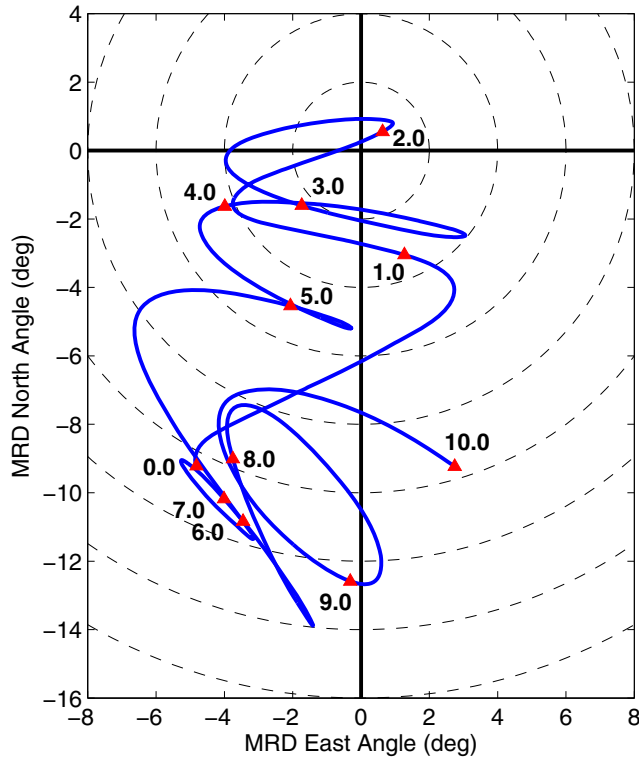


Figure 18 – Phoenix entry body angle with respect to local vertical for the final 10 seconds immediately prior to backshell separation

5. CONCLUSIONS

The examination of the Phoenix inertial measurement unit data has provided insight into the supersonic characteristics of a Viking scaled disk-gap-band parachute in flight conditions that were previously unavailable. The flight data indicate that a significant drag reduction event occurred shortly after the parachute achieved peak load and while the vehicle was still traveling above Mach 1.5. Although an area oscillation is the most likely source of this event, the parachute geometry cannot be confirmed in the absence of any photographic or video data. The authors strongly recommend that an uplook camera be included in all future Mars landed missions that employ a parachute to provide this data. The parachute exhibited neutral lateral stability at supersonic speeds and, in particular, the drag reduction event was associated with a notable lateral translation. In general the lateral motions of the parachute are small at supersonic speeds with excursions of less than eight degrees

away from the anti-velocity direction. The entry body wrist mode is excited by both the unsteadiness of the parachute drag and the lateral motion of the parachute. In general, the Phoenix parachute exhibited good lateral stability in flight that was consistent with Viking era high altitude test data.

The Phoenix Mars Scout mission was directed by the Jet Propulsion Laboratory, California Institute of Technology, under a contract with NASA.

REFERENCES

- [1] Sengupta, A., Kelsch, R., Roeder, J., Werne, M., Witkowski, A., and Kandis, M., "Supersonic Performance of Disk-Gap-Band Parachutes Constrained to a 0-Degree Trim Angle," *Journal of Spacecraft and Rockets*, Vol. 46, No. 6, 2009, pp. 1155-1163.
- [2] Good, P. G. et al., "MRO Imaging of Phoenix Descent," 32nd Annual American Astronautical Society Guidance and Control Conference, Breckenridge, CO, Jan. 30 - Feb. 4, 2009, AAS 09-015.
- [3] Witkowski, A., Kandis, M., and Adams, D. S., "Mars Scout Phoenix Parachute System Performance," AIAA Paper 2009-2907, 2009.
- [4] Dickinson, D., Schlemmer, J., Hicks, F., Michel, F., and Moog, R. D., "Balloon Launched Decelerator Test Program, Post-Flight Test Report, BLDT Vehicle AV 4," NASA CR-112179, 1972.
- [5] Desai, P. N., Prince, J. L., Queen, E. M., Cruz, J. R., and Grover, M. R., "Entry, Descent, and Landing Performance of the Mars Phoenix Lander," AIAA Paper 2008-7346, 2008.
- [6] Adams, D. S., and Crane, E., "Mars Science Laboratory Supersonic Parachute Dynamics," 1st ESA Workshop on Multibody Dynamics for Space Applications, Noordwijk, NL, February 2-3, 2010.

BIOGRAPHY



Douglas Adams is a senior member of the Spacecraft Structures and Dynamics Group at the California Institute of Technology's Jet Propulsion Laboratory in Pasadena, California. His background includes work in structural dynamics, mechanics of materials, fracture mechanics, composite materials, system engineering, and spacecraft attitude dynamics and control. During his ten years at JPL he has worked on numerous programs including the Mars

Exploration Rovers, Terrestrial Planet Finder, MARSIS, SHARAD, and Hydros, and served as the Entry, Descent, and Landing Mechanical Systems Engineer for the Phoenix Mars Scout mission. In his current position he is serving as the Parachute Cognizant Engineer for the Mars Science Laboratory program as well as the Dynamics System Engineer for the Soil Moisture Active Passive (SMAP) rotating radar platform mission.



***Allen Witkowski** currently holds the position of Director of Engineering Operations at Pioneer Aerospace Corporation in South Windsor, CT. Al has been fortunate to be the person responsible for the parachute systems used for every successful landing on the surface of Mars since, and including, Mars Pathfinder in 1997.*

He was the Test Director for the Mars Pathfinder (MPF) Parachute Decelerator Subsystem (PDS) and Program Manager for: Mars Polar Lander, Mars Surveyor 2001, Mars Exploration Rovers, and Mars Scout Phoenix PDS programs. He is currently the Program Manager for the Mars Science Laboratory PDS. He has a BSAE from Embry-Riddle Aeronautical University and has been working on parachute development programs for over 22 years.



***Mike Kandis** currently holds the position of Lead Analytical Engineer and has been with Pioneer Aerospace Corporation since 2002. He has been responsible for the numerical analyses of both the Mars Exploration Rover (MER) and Mars Scout Phoenix (PHX) PDS programs. Mike received his Ph.D. from the University of Texas at Austin in 1999.*

He received his Ph.D. from the University of Texas at Austin in 1999.

